Figure S1

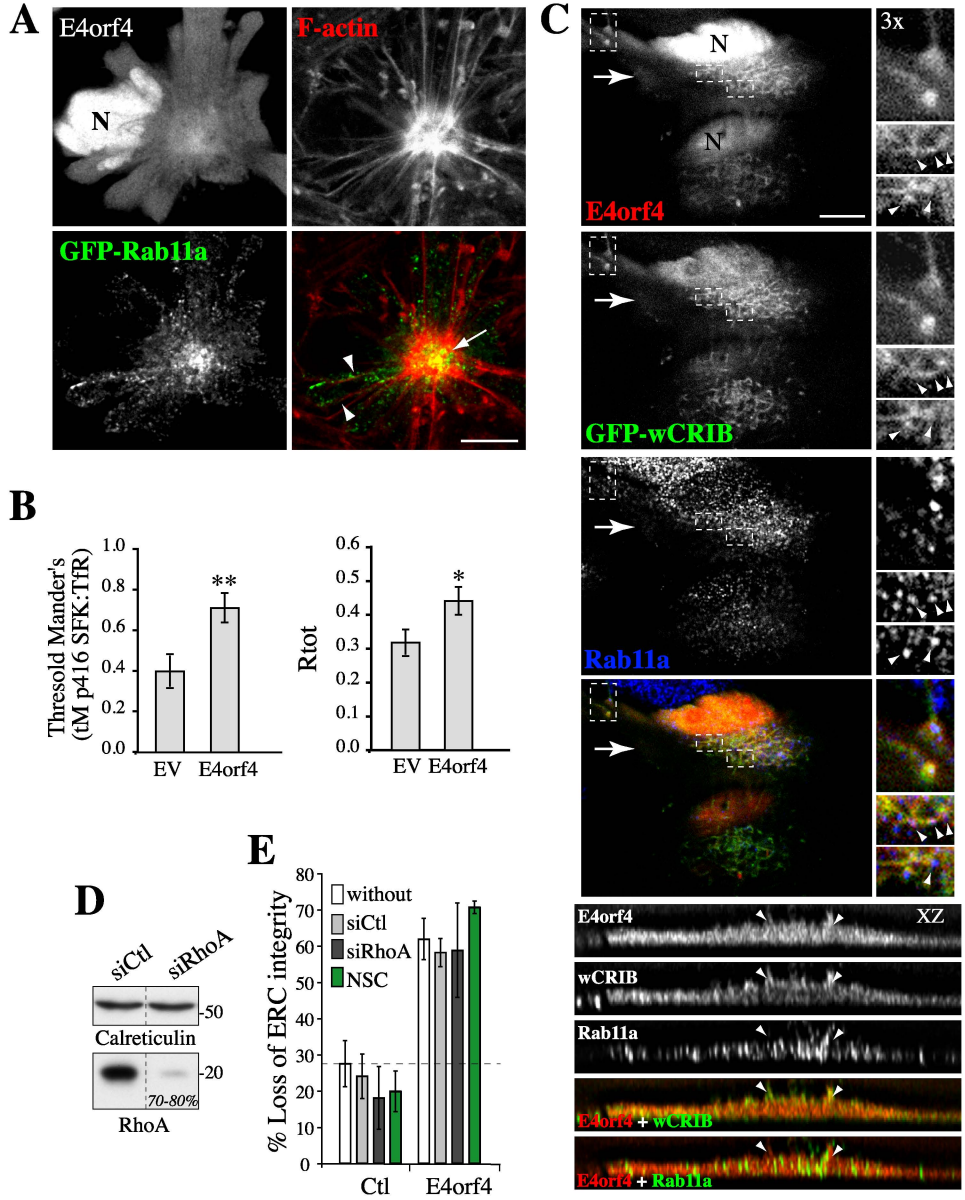
A
E4orf4
N
F-actin
GFP-Rab11a
B
Thresold Mander's (tM p416 SFK:TfR)
1.0
0.8
0.6
0.4
0.2
0.0
**
EV
E4orf4
Rtot
0.6
0.5
0.4
0.3
0.2
0.1
0.0
*
EV
E4orf4
C
N
N
3x
E4orf4
GFP-wCRIB
Rab11a
E4orf4
XZ
wCRIB
Rab11a
E4orf4 + wCRIB
E4orf4 + Rab11a
D
siCtl
siRhoA
50
Calreticulin
20
70-80%
RhoA
E
% Loss of ERC integrity
80
70
60
50
40
30
20
10
0
without
siCtl
siRhoA
NSC
Ctl
E4orf4

Figure S2

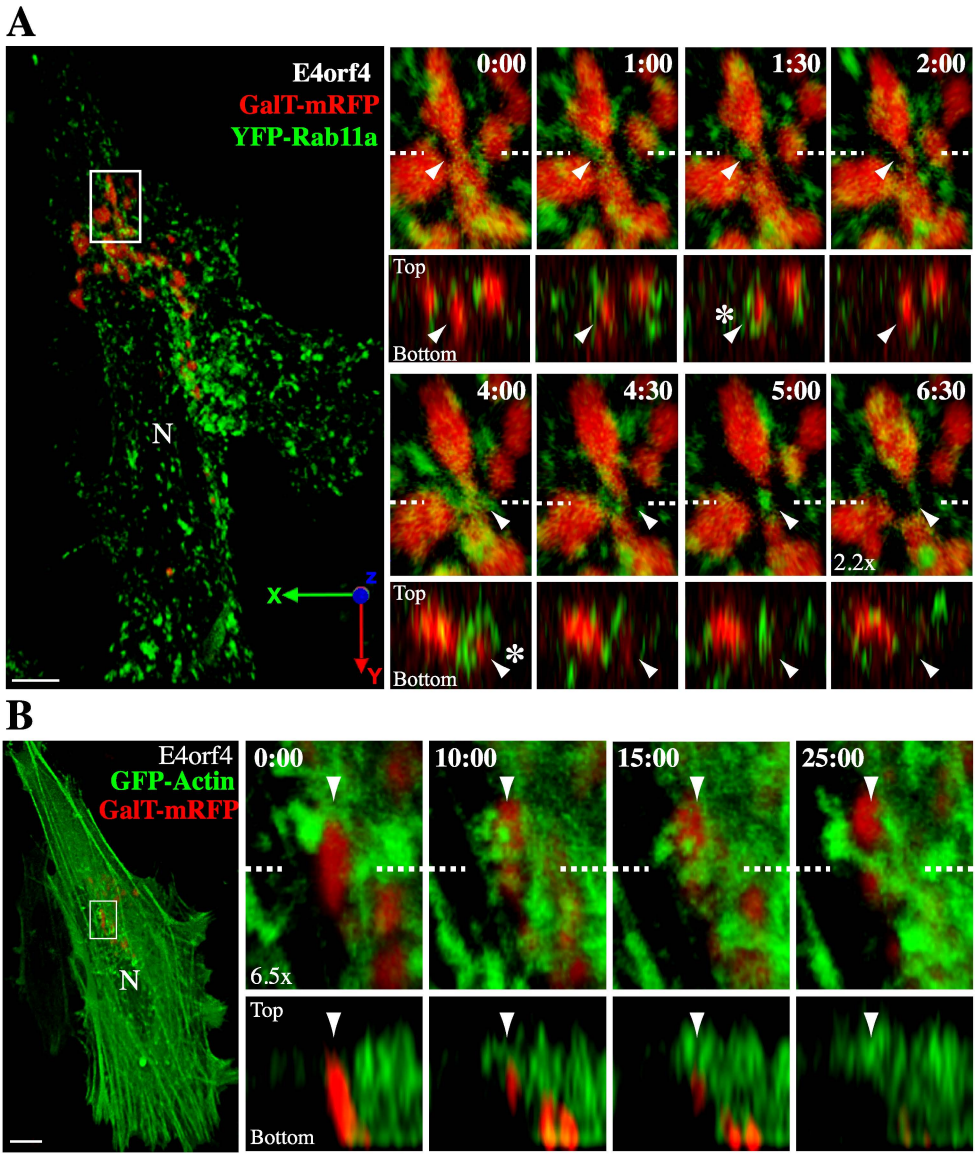
A
E4orf4
GalT-mRFP
YFP-Rab11a
N
X
Z
Y
0:00
1:00
1:30
2:00
Top
Bottom
4:00
4:30
5:00
6:30
2.2x
B
E4orf4
GFP-Actin
GalT-mRFP
N
0:00
10:00
15:00
25:00
6.5x
Top
Bottom

Figure S3

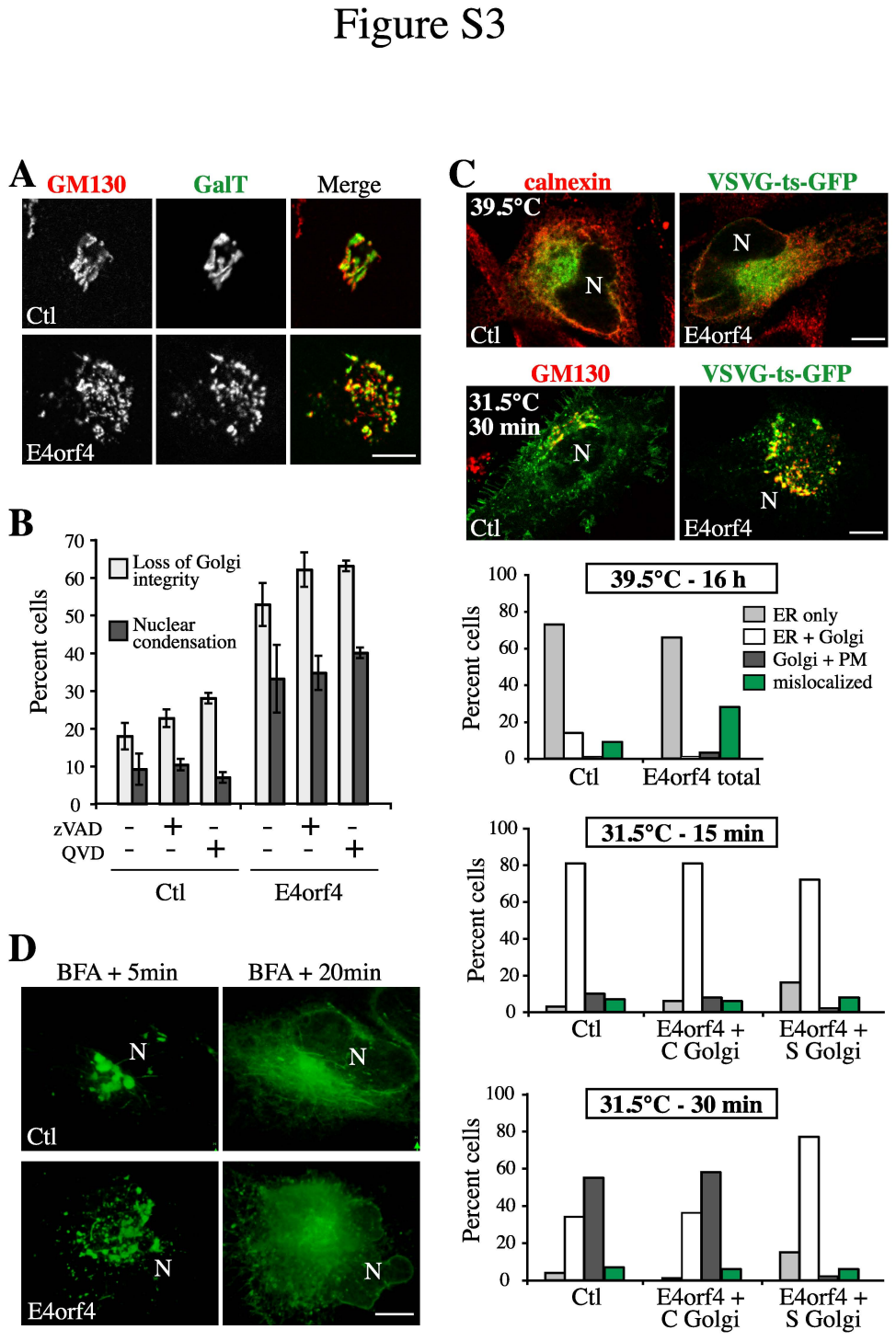
A
GM130
GalT
Merge
Ctl
E4orf4
B
Percent cells
Loss of Golgi integrity
Nuclear condensation
zVAD
QVD
Ctl
E4orf4
C
calnexin
VSVG-ts-GFP
39.5°C
N
Ctl
E4orf4
GM130
VSVG-ts-GFP
31.5°C
30 min
39.5°C - 16 h
ER only
ER + Golgi
Golgi + PM
mislocalized
E4orf4 total
31.5°C - 15 min
E4orf4 + C Golgi
E4orf4 + S Golgi
31.5°C - 30 min
D
BFA + 5min
BFA + 20min

Figure S4

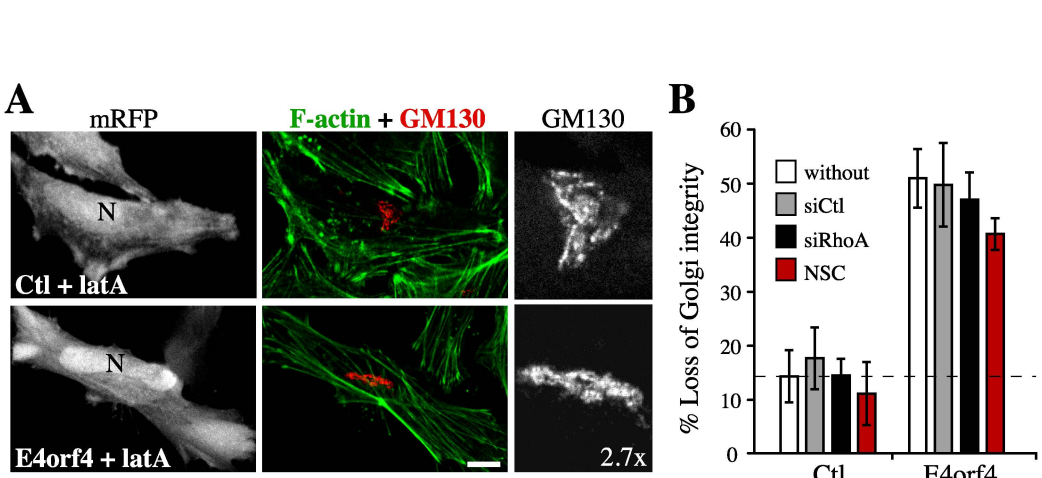
A
mRFP
F-actin + GM130
GM130
N
Ctl + latA
N
E4orf4 + latA
2.7x
B
% Loss of Golgi integrity
60
50
40
30
20
10
0
without
siCtl
siRhoA
NSC
Ctl
E4orf4

Figure S5

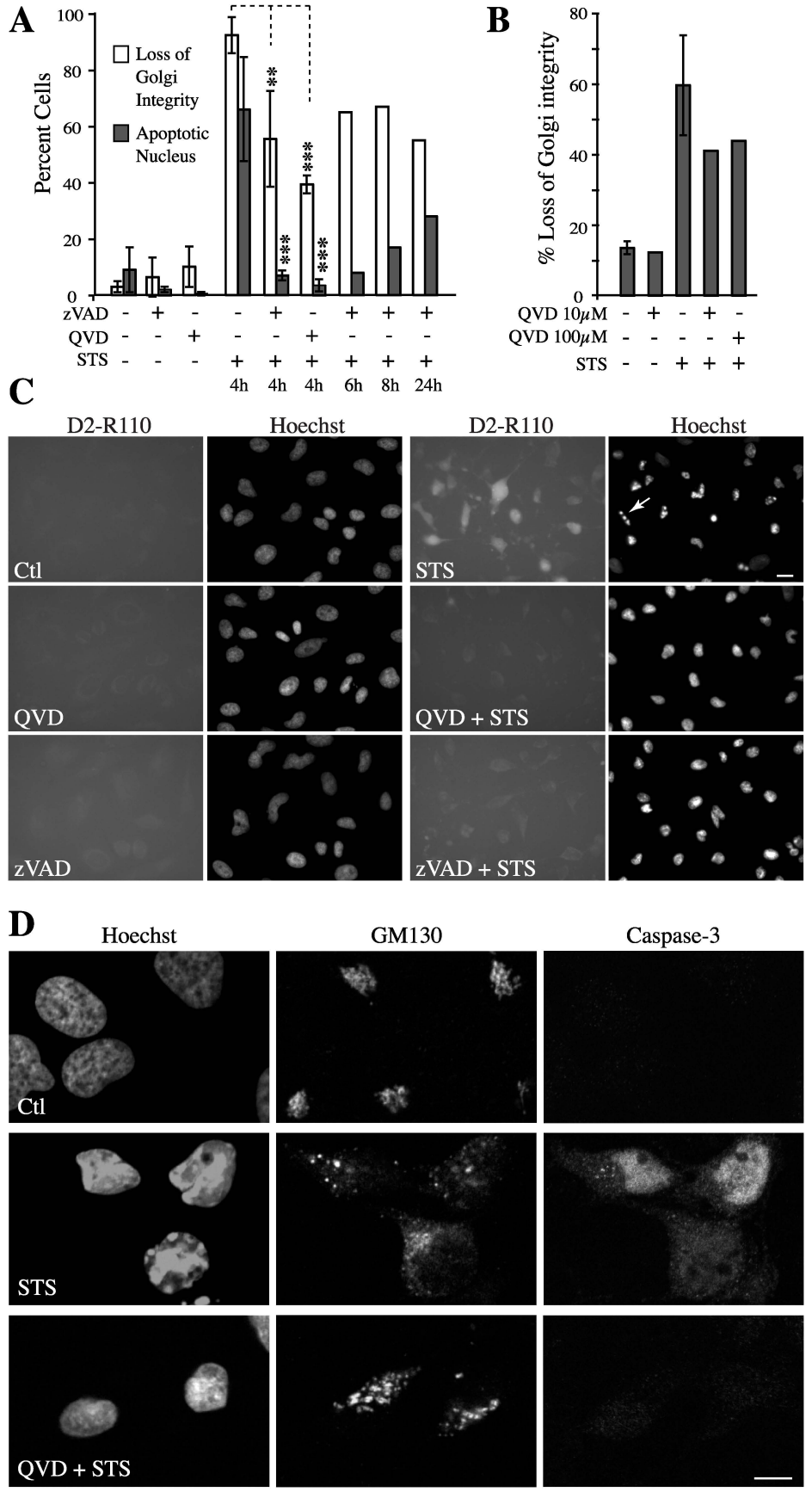
A
Percent Cells
Loss of Golgi Integrity
Apoptotic Nucleus
zVAD
QVD
STS
4h
4h
4h
6h
8h
24h
B
% Loss of Golgi integrity
QVD 10μM
QVD 100μM
STS
C
D2-R110
Hoechst
D2-R110
Hoechst
Ctl
STS
QVD
QVD + STS
zVAD
zVAD + STS
D
Hoechst
GM130
Caspase-3
Ctl
STS
QVD + STS

Figure S1. **(A) Polarization of REs to the peri-Golgi region correlates with the assembly of a juxtanuclear contractile network in response to E4orf4.** Single plane views of a representative Hela cell transfected with E4orf4-mRFP and GFP-Rab11a, showing the massive recruitment of REs to the juxtanuclear actin-myosin ring (arrow; F-actin staining with phalloidin) and along the emerging actin cables (arrowheads) which takes place concomitantly with dramatic changes in cell morphology. N, cell nucleus; Bar, 10μm. **(B) E4orf4 promotes SFK signaling at REs.** Quantitative analysis of coincident pixels between phospho-SFK and TfR staining was performed using the "colocalisation threshold" plugin of ImageJ. Graphs show the threshold-ajusted Manders's coefficient (tM) of phospho-Src over TfR and the Pearson's index of overall colocalization (Rtot). Data are the means ±SE from 8 cells. **(C) E4orf4 and active Cdc42 co-distribute within tail- and coat-like structures associated with REs, concomitantly with ERC disruption.** Single plane views and XZ reconstructions of deconvolved confocal z-stacks of representative Hela cells transfected with E4orf4-mRFP and GFP-wCRIB, showing the overlapping distributions of E4orf4 and wCRIB in tail and coat-like structures associated with REs as seen by Rab11a staining. Arrowheads in enlarged images of the boxed regions and in XZ views designate structures labeled by E4orf4 and wCRIB, which embed Rab11a endosomes. Arrows indicate the X axis. N, nucleus; Bar, 10 μm. **(D, E) ERC structural changes in response to E4orf4 do not depend on RhoA and Rac1.** (D) Western blots of Hela cell extracts harvested 72 h after transfection with the indicated siRNAs. The estimated percentage of reduction of RhoA protein level is indicated; calreticulin: loading controls. Dividing lines indicate grouping of images from parts of the same gel. (E) Graph depicts the percentages of Hela and MCF7 cells, which have been transfected with the indicated siRNAs or exposed to the Rac1 inhibitor NSC23766 (NSC, 100 μM) before transfection of GFP-Rab11a together with mRFP

(Ctl) or E4orf4-mRFP, which show loss of ERC integrity. The dashed line delineates the background level of ERC dispersal in control cells. Data are the means ±SD of 2 experiments, n> 200 cells.

Figure S2: **(A) Spatially restricted RE-Golgi interactions are coupled to cycles of Golgi membrane stretching and fission.** 3D reconstruction of confocal image stacks of a representative Hela cell transfected with Flag-E4orf4, GalT-mRFP (TGN) and YFP-Rab11a (RE) which exhibits ERC fragmentation and partial disassembly of the Golgi. Confocal z-sections were taken at ≥ 30 s intervals, and enlarged 3D-time sequences of the boxed region show 2 cycles of RE-Golgi membrane associations (asterisks) followed by fission of a Golgi element that had already undergone stretching at this site (arrowhead). XZ-views of the corresponding Golgi area confirm the spatial superposition of RE and Golgi membranes (dotted lines:X axis). N, nucleus; Bar, 10 μm. **(B) Remodeling of Golgi membranes is associated with actin assembly at the site of membrane fission.** 3D reconstruction of a representative Hela cell transfected with Flag-E4orf4, GalT-mRFP and GFP-actin. Enlarged images of the boxed region show the 3D-sequence from confocal z-sections acquired at 5 min intervals (Supplemental Video 2). XZ-views of a Golgi element (arrowhead) confirm the spatial and temporal superposition of actin structures and Golgi membranes at sites of stretching and fission (dotted lines indicate X axis). N, nucleus; Bar, 10 μm.

Figure S3. **(A) Scattered Golgi fragments in E4orf4-expressing cells contain *cis* and *trans* Golgi markers.** Single plane views of Hela cells transfected with GalT-GFP together with mRFP (Ctl) or E4orf4-mRFP, showing co-distribution of *cis* (GM130 staining) and medial-*trans* Golgi (GalT-GFP) markers in the scattered Golgi fragments of a E4orf4-positive cell. **(B) Golgi**

membrane scattering precedes nuclear condensation in response to E4orf4 and is caspase-independent. Graph depicts the percentages of Hela cells which show loss of Golgi integrity (GM130 staining) and nuclear condensation (Hoechst staining) 24 h after transfection of mRFP (Ctl) or E4orf4-mRFP and growth in the presence (+) or absence (-) of wide-spectrum caspase inhibitors. Data are the means ±SD of at least 2 experiments, n≥200 cells. **(C, D) Golgi membrane scattering in response to E4orf4 is associated with a selective block of Golgi-to-plasma membrane protein transport.** Hela cells were transfected with VSVG-ts-GFP and mRFP (Ctl) or E4orf4-mRFP. Cells incubated overnight at the restrictive temperature (39.5°C) were kept at 39.5°C or shifted to the permissive temperature (31.5°C) in the presence of cycloheximide (75 μM) for 15 or 30 min. **(C)** Single plane views showing staining of the endoplasmic reticulum (ER, calnexin) and *cis* Golgi (GM130) in control (Ctl) *versus* E4orf4 cells. N, nucleus; Bar, 10 μm. Graphs depict the percentages of control and E4orf4-positive cells with either compact (C Golgi) or scattered (S Golgi) Golgi membranes that displayed VSVG protein in the indicated cell compartment, as estimated by immunostaining using appropriate markers. Green bars represent the proportion of cells bearing VSVG protein throughout the cell when the level of expression was too high (mislocalized) **(D)** Control (Ctl) or E4orf4-expressing cells that had accumulated VSVG-ts-GFP in the Golgi after an overnight incubation at 39.5°C followed by a shift to 31.5°C for 30 min in the presence of cycloheximide, were exposed to BFA to stimulate a massive Golgi-to-ER retrograde transport of membranes. Confocal z-sections were taken at 5 min intervals following BFA addition. Representative 3D reconstructions of image stacks show no significant inhibition of VSVG protein retrieval into the ER in E4orf4-expressing cells. Bar, 10 μm.

Figure S4. **Loss of Golgi integrity relies on actin dynamics, but not on RhoA or Rac1.** (A) Single plane views of Hela cells transfected with mRFP (Ctl) or E4orf4-mRFP and exposed to a low concentration of LatA (0.5 μM in DMSO) that inhibited actin dynamics without inducing a complete disruption of the actin cytoskeleton (phalloidin), or to DMSO alone. GM130 staining revealed a marked protection of Golgi structural integrity in E4orf4-expressing cells treated with LatA. N, nucleus; Bar, 10 μm. (B) Graph depicts the percentages of mRFP (Ctl) and E4orf4-mRFP-expressing cells transfected with the indicated siRNAs or exposed to the Rac1 inhibitor NSC23766 (NSC) which show a loss of Golgi integrity, as seen by GM130 staining; means ±SD of at least 3 experiments, n> 300 cells.

Figure S5: **Apoptotic Golgi disassembly in response to STS only partially depends on caspases** (A) Hela cells were exposed to STS or to the vehicle alone for the indicated time in the presence (+) or absence (-) of a wide spectrum caspase inhibitor (zVAD-fmk or QVD-OPh). Graph depicts the percentages of cells, which display loss of Golgi integrity and nuclear condensation as revealed by GM130 and Hoechst staining, respectively. Data are the means ±SD of 3 experiments, n >500 cells. (B) The graph shows that a 10-fold increase in the concentration of QVD-OPh (100 μM) does not potentiate its partial inhibitory effect on STS-induced Golgi membrane scattering. Of note, 100 μM QVD-OPh has been shown to completely inhibited caspase-2-mediated cell death of neurons, in contrast to other poly-caspase inhibitors (z-VAD-fmk, Boc-D-fmk) that poorly inhibit caspase-2 (Chauvier *et al*., 2007). (C) Hela cells were exposed to STS for 4 h in the presence or absence of a wide spectrum caspase inhibitor (zVAD-fmk, 50 μM or QVD-OPh, 10 μM) and incubated with a generic caspase substrate covalently linked to rhodamine 110 (D2-R110), whose cleavage by caspases increases R110 fluorescence.

Representative epifluorescence images show that STS-induced caspase activities (D2-R110 fluorescence intensity) were efficiently reduced by caspase inhibitors in most cells especially by QVD-OPh, along with apoptotic nuclear fragmentation (Hoechst staining, arrow) (D) Confocal images of control Hela cells or Hela cells exposed to STS for 4 h in the presence or absence of QVD-OPh, which show that cells exhibit persistent Golgi membrane scattering in the presence of QVD-OPh without acute caspase-3 activation (staining for active caspase-3). Bar, 10μm.

Video 1. 3D-video microscopy of a representative Hela cell transfected with Flag-E4orf4 (not shown), YFP-Rab11a (green) and GalT-mRFP (red) showing a dynamic interaction between YFP-Rab11a-labeled RE and GalT-mRFP-labeled Golgi membranes that coincides with the stretching and fission of the Golgi element at the same site. Confocal z-sections (0.5 μm) covering the entire depth of the cell were acquired at 10 sec intervals over a 2 min-period and are displayed at 7 frames/sec. This video is related to Figure 5A.

Video 2. 3D-video microscopy of a representative Hela cell transfected with Flag-E4orf4 (not shown), GalT-mRFP (red) and GFP-actin (green) showing the local remodeling of GalT-mRFP-labeled Golgi elements that occurs concomitantly with the emergence of actin structures at the same site. Confocal z-sections (0.5 μm) covering the entire depth of the cell were acquired at 5 min intervals over a 35 min-period and are displayed at 7 frames/s. This video is related to Supplemental Figure 2B.

SUPPLEMENTAL MATERIALS

Expression Vectors- GalT-mRFP (a.a 1-60 of Galactosyltransferase) was produced by subcloning the BamHI/EcoRI fragment of mRFP from pRSETB-mRFP (Dr. Tsien, La Jolla, USA) into the BamHI/EcoRI sites of GalT-CFP (Nichols *et al*., 2001). The pmRFP-C was generated by replacing the GFP cDNA from pEGFP-C1 (Clonetech) with the PinAI/BglII mRFP fragment obtained by PCR amplification from pRSETB-mRFP. The mRFP-actin was produced by subcloning the XhoI/PstI cDNA fragment from GFP-actin (Choidas *et al*., 1998) into the BglII/PstI sites of pmRFP-C (Robert *et al*., 2006).

Quantitative analyses of coincidence between phospho-SFKs-labelled structures and REs- The relative distribution of p416 SFK (green fluorescent signal) to REs (TfR staining, red fluorescent signal) was analyzed using deconvolved confocal images by 2 different approaches. To measure the coincidence between fluorescent subcellular structures within a cell, we used the Volocity 5.0 to perform an object-based analysis as described (Bolte and Cordelieres, 2006). Fluorescent objects in both channels were found by applying a threshold set at 800 a.u. or greater and objects were delineated using a segmentation procedure based on a watershed algorithm. The intersecting area between objects with a size volume ≥ 3 voxels in the green channel (phospho-SFKs) and those in the red channel (REs) was determined and was expressed as the ratio in percent of the area of green voxels that overlap with the area of red voxels over the total area of green voxels. As a complementary approach, individual pixel coincidence analysis was performed using the "colocalization threshold" plugin in ImageJ (http://www.uhnresearch.ca/facilities/wcif/software/Plugins/colocalisation_threshold.html) which

uses the Coste's threshold algorithm for determining automatic threshold (Costes *et al*., 2004). Confocal image stacks were cleared of background using a region of interest (ROI) outside cells with the "substract background from ROI" function and filtered with a median filter to remove point noise. The single channel specific threshold-adjusted Mander's coefficient (tM) provides a good indicator of the proportion of the green signal (phospho-SFK) coincident with the signal in the red channel (REs) over its total intensity, which may even be used if the intensities in both channels are different from one another. The Pearson's index (Rtot) gives an estimation of the linear relationship fluorescence intensity pixels of green and red image pairs and is more sensitive to individual channel intensity.

Quantitative analyses of organelle's dynamic changes- Structural integrity of the ERC was monitored routinely in both MCF7 and Hela cells by confocal microscopy. In MCF7 cells, ERC markers are concentrated to the pericentrosomal region of the cell and "loss of ERC integrity" was estimated by scoring the number of cells that exhibited lost of ERC-marker proteins (Rab11a, TfR) from the pericentrosomal region by visual inspection of fixed specimens using a 60x oil 1.4 NA objective. In Hela cells, ERC-marker proteins show a more loose distribution throughout the cytoplasm to typical tubular endosomes. In these cells, "loss of ERC integrity" was estimated on the basis of fragmentation of ERC tubules by scoring the number of cells that exhibited a predominant staining of ERC-marker proteins to shorter and discontinuous ERC-derived vesicular structures by analysis of 3D reconstructions of confocal image stacks of representative cells. "Loss of Golgi integrity" was estimated based on the scattering of >50% of Golgi membranes (>50% short discontinuous Golgi elements) by visual inspection of fixed specimens using a 60x

oil 1.4 NA objective. The nuclear morphology was analyzed by epifluorescence microscopy and considered typical of dying cells on the basis of intense chromatin condensation and nuclear shrinkage (<50% of interphase nucleus volume, caspase-independent) and/or nuclear fragmentation (STS, caspase-dependent).

Table S1. Expression vectors previously described and chemicals used in this study

Expression vector	**Reference**
Flag-E4orf4-mRFP (WT, 6R-A and 4Y-F)	(Robert *et al*., 2006)
Flag-E4orf4	(Champagne *et al*., 2004)
myc-Cdc42	(Lamarche *et al*., 1996)
GFP-Rab11a	(Hunyady *et al*., 2002)
YFP-Rab11a	(Sonnichsen *et al*., 2000)
golgin-160-GFP	(Mancini *et al*., 2000)
golgin-84-GFP	(Diao *et al.*, 2003)
VSVG-ts-GFP	(Presley *et al*., 1997)
GFP-wCRIB	(Moreau *et al*., 2000)
chicken c-Src	(Thomas *et al*., 1991)
Chemicals	**Source**
Brefeldin A	Sigma-Aldrich
D2-R110	Molecular Probes
Latrunculin A	Calbiochem/EMD
NSC23766	
PP2	
Q-VD-OPh	
SKI-1	
Staurosporin	
SU6656	
zVAD-fmk	

Table S2. Antibodies and siRNA oligonucleotides used in this study

Antibody	**Antibody Type**	**Source**
ß-actin (AC15 ou AC-74)	Mouse monoclonal	Sigma-Aldrich
Calnexin (clone C8.B6)	Mouse monoclonal	Millipore
Calreticulin	Mouse monoclonal	BD Biosciences
Cleaved Caspase-3 (Asp175)	Rabbit polyclonal	Cell SignalingTechnology
Cdc42 (P1)	Rabbit polyclonal	Santa Cruz Biotechnologies,
Flag (M2)	Mouse monoclonal	Sigma-Aldrich
Fyn (clone 25)	Mouse monoclonal	BD Biosciences
GAPDH (clone 6C5)	Mouse monoclonal	Fitzgerald Industries International
GM130 (clone 35)	Mouse monoclonal	BD Biosciences
Golgin-97 (clone CDF4)	Mouse monoclonal	Molecular Probes/Invitrogen
MHCI (clone W6/32)	Mouse monoclonal	AbD Serotec / MorphoSys
Phosphotyrosines (PY20)	Mouse monoclonal	ICN/MP Biochemicals
Rab11a	Rabbit polyclonal	Zymed Laboratories
RhoA (clone 55)	Mouse monoclonal	BD Biosciences
v-Src (Ab1)	Mouse monoclonal	Calbiochem/EMD
Phospho-Src Family (Tyr416)	Rabbit polyclonal	Cell SignalingTechnology,
Syntaxin 6	Mouse monoclonal	BD Biosciences
Transferrin Receptor (clone H68.4)	Mouse monoclonal	Zymed Laboratories
Yes (clone 1)	Mouse monoclonal	BD Biosciences
Targeted protein	**siRNA**	**Source**
GFP	GFP-22 siRNA 3'-labelled with Rhodamine	QIAGEN
Negative Control	AllStars Negative Control siRNA	QIAGEN
Human Cdc42	Hs_CDC42_1_HP siRNA	QIAGEN
	Hs_CDC42_4_HP siRNA	
Human Fyn	Hs_FYN_7_HP siRNA	QIAGEN
Human Rab11a	Rab11a #1 siRNA	(Wilson *et al*., 2005)
	Rab11a #2 siRNA (siGenome SMARTPool)	Dharmacon
Human RhoA	Hs_RHOA_1_HP Validated	QIAGEN
Human Src	Hs_SRC_7_HP Validated	QIAGEN
Human syntaxin 6	Hs_STX6_9	QIAGEN
Human Yes	Hs_YES_7_HP Validated	QIAGEN

References

Bolte, S., and Cordelieres, F.P. (2006). A guided tour into subcellular colocalization analysis in light microscopy. J Microsc *224*, 213-232.

Champagne, C., Landry, M.C., Gingras, M.C., and Lavoie, J.N. (2004). Activation of adenovirus type 2 early region 4 ORF4 cytoplasmic death function by direct binding to Src kinase domain. J Biol Chem *279*, 25905-25915.

Chauvier, D., Ankri, S., Charriaut-Marlangue, C., Casimir, R., and Jacotot, E. (2007). Broad-spectrum caspase inhibitors: from myth to reality? Cell Death Differ *14*, 387-391.

Choidas, A., Jungbluth, A., Sechi, A., Murphy, J., Ullrich, A., and Marriott, G. (1998). The suitability and application of a GFP-actin fusion protein for long-term imaging of the organization and dynamics of the cytoskeleton in mammalian cells. Eur J Cell Biol *77*, 81-90.

Costes, S.V., Daelemans, D., Cho, E.H., Dobbin, Z., Pavlakis, G., and Lockett, S. (2004). Automatic and quantitative measurement of protein-protein colocalization in live cells. Biophys J *86*, 3993-4003.

Diao, A., Rahman, D., Pappin, D.J., Lucocq, J., and Lowe, M. (2003). The coiled-coil membrane protein golgin-84 is a novel rab effector required for Golgi ribbon formation. J Cell Biol *160*, 201-212.

Hunyady, L., Baukal, A.J., Gaborik, Z., Olivares-Reyes, J.A., Bor, M., Szaszak, M., Lodge, R., Catt, K.J., and Balla, T. (2002). Differential PI 3-kinase dependence of early and late phases of recycling of the internalized AT1 angiotensin receptor. J Cell Biol *157*, 1211-1222.

Lamarche, N., Tapon, N., Stowers, L., Burbelo, P.D., Aspenstrom, P., Bridges, T., Chant, J., and Hall, A. (1996). Rac and Cdc42 induce actin polymerization and G1 cell cycle progression independently of p65PAK and the JNK/SAPK MAP kinase cascade. Cell *87*, 519-529.

Mancini, M., Machamer, C.E., Roy, S., Nicholson, D.W., Thornberry, N.A., Casciola-Rosen, L.A., and Rosen, A. (2000). Caspase-2 is localized at the Golgi complex and cleaves golgin-160 during apoptosis. J Cell Biol *149*, 603-612.

Moreau, V., Frischknecht, F., Reckmann, I., Vincentelli, R., Rabut, G., Stewart, D., and Way, M. (2000). A complex of N-WASP and WIP integrates signalling cascades that lead to actin polymerization. Nat Cell Biol *2*, 441-448.

Nichols, B.J., Kenworthy, A.K., Polishchuk, R.S., Lodge, R., Roberts, T.H., Hirschberg, K., Phair, R.D., and Lippincott-Schwartz, J. (2001). Rapid cycling of lipid raft markers between the cell surface and Golgi complex. J Cell Biol *153*, 529-541.

Presley, J.F., Cole, N.B., Schroer, T.A., Hirschberg, K., Zaal, K.J., and Lippincott-Schwartz, J. (1997). ER-to-Golgi transport visualized in living cells. Nature *389*, 81-85.

Robert, A., Smadja-Lamere, N., Landry, M.C., Champagne, C., Petrie, R., Lamarche-Vane, N., Hosoya, H., and Lavoie, J.N. (2006). Adenovirus E4orf4 hijacks rho GTPase-dependent actin dynamics to kill cells: a role for endosome-associated actin assembly. Mol Biol Cell *17*, 3329-3344.

Sonnichsen, B., De Renzis, S., Nielsen, E., Rietdorf, J., and Zerial, M. (2000). Distinct membrane domains on endosomes in the recycling pathway visualized by multicolor imaging of Rab4, Rab5, and Rab11. J Cell Biol *149*, 901-914.

Thomas, J.E., Soriano, P., and Brugge, J.S. (1991). Phosphorylation of c-Src on tyrosine 527 by another protein tyrosine kinase. Science *254*, 568-571.

Wilson, G.M., Fielding, A.B., Simon, G.C., Yu, X., Andrews, P.D., Hames, R.S., Frey, A.M., Peden, A.A., Gould, G.W., and Prekeris, R. (2005). The FIP3-Rab11 protein complex regulates

recycling endosome targeting to the cleavage furrow during late cytokinesis. Mol Biol Cell *16*, 849-860.